Molecular Therapy
Oncolytics
Original Article

AMERICAN SOCIETY of GENE & CELL THERAPY

Two-Dimensional Regulation of CAR-T Cell Therapy with Orthogonal Switches

MyLinh T. Duong,[1] Matthew R. Collinson-Pautz,[1] Eva Morschl,[1] An Lu,[1] Slawomir P. Szymanski,[1] Ming Zhang,[1] Mary E. Brandt,[1] Wei-Chun Chang,[1] Kelly L. Sharp,[1] Steven M. Toler,[1] Kevin M. Slawin,[1] Aaron E. Foster,[1] David M. Spencer,[1] and J. Henri Bayle[1]

[1]Bellicum Pharmaceuticals, 2130 W. Holcombe Blvd., Suite 800, Houston, TX 77030, USA

Use of chimeric antigen receptors (CARs) as the basis of targeted adoptive T cell therapies has enabled dramatic efficacy against multiple hematopoietic malignancies, but potency against bulky and solid tumors has lagged, potentially due to insufficient CAR-T cell expansion and persistence. To improve CAR-T cell efficacy, we utilized a potent activation switch based on rimiducid-inducible MyD88 and CD40 (iMC)-signaling elements. To offset potential toxicity risks by this enhanced CAR, an orthogonally regulated, rapamycin-induced, caspase-9-based safety switch (iRC9) was developed to allow *in vivo* elimination of CAR-T cells. iMC costimulation induced by systemic rimiducid administration enhanced CAR-T cell proliferation, cytokine secretion, and antitumor efficacy in both *in vitro* assays and xenograft tumor models. Conversely, rapamycin-mediated iRC9 dimerization rapidly induced apoptosis in a dose-dependent fashion as an approach to mitigate therapy-related toxicity. This novel, regulatable dual-switch system may promote greater CAR-T cell expansion and prolonged persistence in a drug-dependent manner while providing a safety switch to mitigate toxicity concerns.

INTRODUCTION

Chimeric antigen receptor (CAR)-based T cell therapies, comprising an extracellular tumor antigen binder fused to one or more cytosolic signaling domains, have proven highly effective for a relatively narrow range of target indications, particularly $CD19^+$ B cell leukemias and lymphomas[1–6] and $BCMA^+$ multiple myeloma.[7] These clinical successes have supported expanding the use of CAR-T cells due to their highly target-specific mode of action and curative potential. However, CAR-T cell efficacy against solid tumors has remained largely elusive.[8–11] In addition to robust CAR-T cell expansion, eradication of solid tumors may also require durable persistence and sufficient costimulation to resist T cell exhaustion.

To increase T cell potency[12–17] and persistence, most CARs incorporate costimulatory signaling domains, derived from CD28 or 4-1BB (CD137), presented in tandem with T cell receptor (TCR) ζ-chain-encoded immunoreceptor tyrosine activation motifs (ITAMs).[14,16,18,19] Moreover, the 4-1BB costimulatory domain appears to promote prolonged T cell persistence *in vivo* relative to first-generation and CD28-containing CARs,[20,21] a feature that could further delay relapse, but it provides no remote control of this expansion once cells are infused. As a potentially safer and more effective alternative, we recently demonstrated that inducible MyD88/CD40 (iMC)[22] could provide controlled costimulation to CAR-T cells, increasing their proliferation, survival, and antitumor efficacy against hematological and solid tumor models, following *in vivo* administration of the homodimerizing drug rimiducid.[17,23] Rimiducid (Rim, formerly known as AP1903) has two symmetrical surfaces that bind with high ($K_d \sim 0.1$ nM) affinity to the F36V variant of FKBP12 (Fv), leading to oligomerization of iMC and co-induction of MyD88 and CD40 signaling.[24,25] This results in robust ligand-dependent induction of nuclear factor κB (NF-κB) and other transcription factors.[22,26]

While stronger costimulation can dramatically improve tumor control, severe adverse events, principally from cytokine release syndrome or autoreactivity, are often observed in the clinic following CAR-T cell treatment of hematopoietic malignancies.[1] To mitigate toxicity, pro-apoptotic safety switches have been devised using FKBP-based dimerizers,[27–32] including clinically validated iCaspase-9 (iC9),[29] which triggers rapid, cell cycle-independent and non-inflammatory cell-autonomous apoptosis of iC9-gene-modified cells following the administration of activating ligand.[27,31] iC9 is a fusion of Fv with a truncated allele of caspase-9, lacking its caspase recruitment domain (CARD) to minimize basal signaling.

While iMC and iC9 confer effective control of two critical and disparate aspects of CAR-T cell function, both rely on triggering by the same ligand, Rim. Thus, to simultaneously incorporate safety

Received 13 November 2018; accepted 15 December 2018;
https://doi.org/10.1016/j.omto.2018.12.009.

Correspondence: David M. Spencer, Bellicum Pharmaceuticals, 2130 W. Holcombe Blvd., Suite 800, Houston, TX 77030, USA.
E-mail: dspencer@bellicum.com
Correspondence: J. Henri Bayle, Bellicum Pharmaceuticals, 2130 W. Holcombe Blvd., Suite 800, Houston, TX 77030, USA.
E-mail: jhbayle@bellicum.com

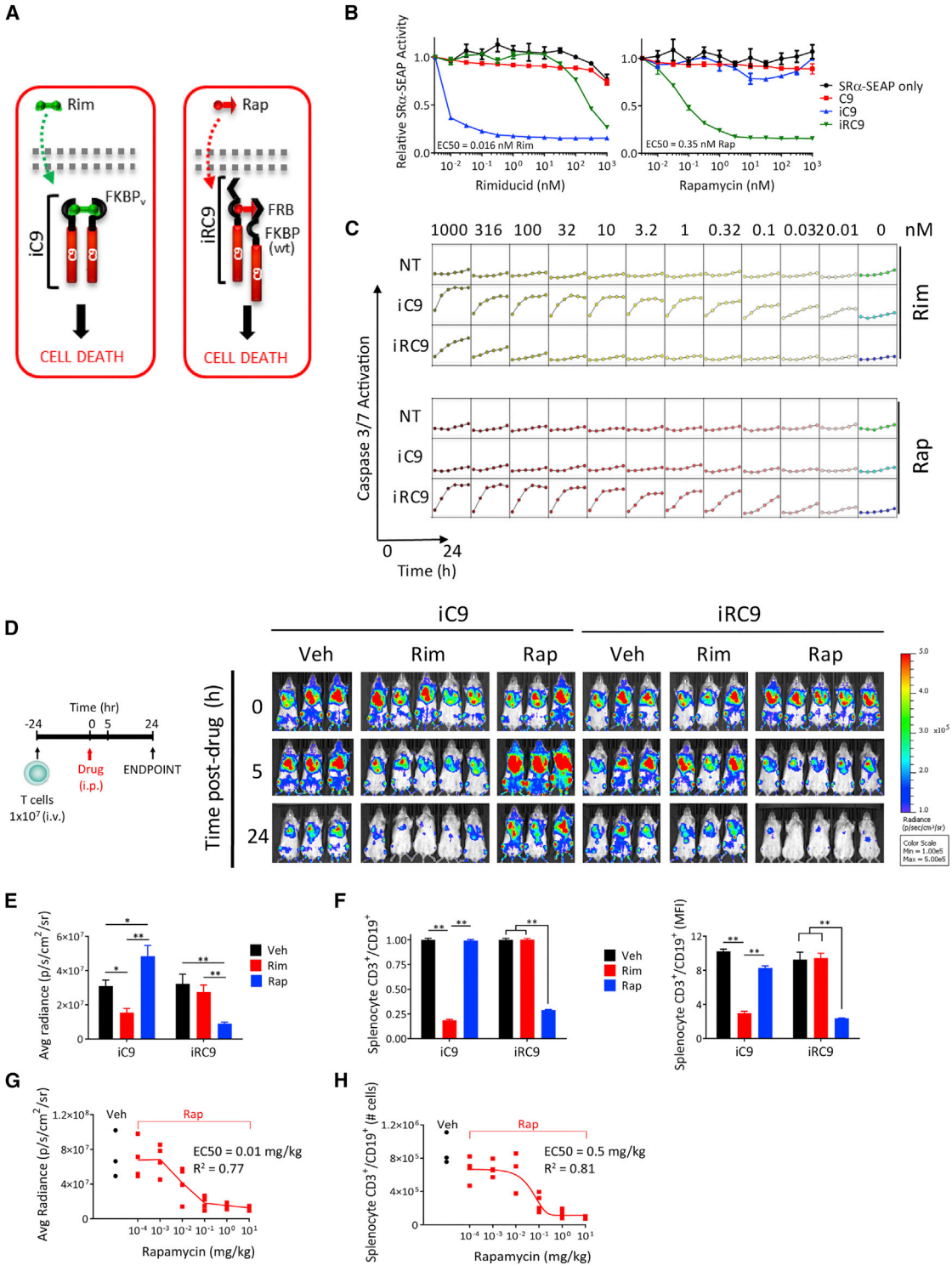

Figure 1. Development of a Rap-Inducible Pro-apoptotic Switch

(A) Schematic of rimiducid (Rim)- and rapamycin (Rap)-regulated inducible caspase-9 (iC9 and iRC9, respectively). (B) Reporter assay of induced apoptosis in transfected HEK293 cells, measured as reduced constitutively produced SeAP reporter activity at 18 h post-stimulation. (C) HEK293 apoptosis determined by an IncuCyte/caspase-3 and -7 assay. Caspase-3 and -7 reporter substrate (2 μM) was added to non-transduced (NT) or iC9- or iRC9-transfected cells at the time of drug treatment as indicated, and fluorescence was monitored in real time at 4-h intervals. (D) Ligand specificity *in vivo* of the iC9 and iRC9 switches. Activated PBMCs were co-transduced with EGFPFluc and

(legend continued on next page)

and costimulation within the same CAR-T cell platform, a second distinct switching mechanism is required. Due to the extended persistence favored by non-immunogenic human proteins, we used a rapamycin (Rap)-based dimerizer system as the basis of this second switch. When chronically administered, Rap is a potent immunosuppressant and antiproliferative agent that acts mechanistically as a protein heterodimerizer, linking FKBP12 with the kinase mTOR.[33–35] Several molecular switches have been devised using the 89-amino acid FKBP-Rap binding (FRB) domain of mTOR[36] and FKBP12 to dimerize signaling proteins fused to each binding domain.[37–41] Because Rap-directed dimerization is asymmetric, the simplest Rap-based binary switch would require two distinct polypeptides. However, to minimize the genetic payload and improve protein expression, herein we present a straightforward technique in which both FRB and FKBP12 are fused in-frame with caspase-9 to generate a Rap-induced, caspase-9-based safety switch (iRC9), which allows Rap to dimerize two or more iRC9 molecules, leading to apoptosis. Thus, the incorporation of iRC9 and iMC, together with a first-generation CAR, generates the first reported dual-switch (DS) CAR-T cell, capable of regulated costimulation to drive CAR-T cell expansion and activity while retaining an orthogonally regulated switch to ensure safety.

RESULTS

Rap-Dependent Activation of an iRC9 Apoptosis Switch in T Cells

iRC9 comprises an FKBP12 (107 amino acids) followed by an FRB domain (89 amino acids [aas]) and Δcaspase-9. Rap-regulated iRC9 was designed to be triggered by drug binding to the FKBP12 of one iRC9 and recruitment of the FRB domain of a second iRC9, leading to dimerization and activation of caspase-9 (Figure 1A). Although signaling proteins are fused to FKBP12 in both Rap- and Rim-based switches, we postulated that the exquisite allele specificity of Rim for the Fv variant of FKBP12 in iMC would permit orthogonal use of distinct FKBP12-based signaling switches. Fv substitutes phenylalanine at amino acid 36 (F36) within the drug-binding pocket with a more compact valine (V36). Specificity for Rim thus results from the substitution of an ethyl group for the F36-interacting carbonyl present at C9 of FK506 and C14 of Rap, increasing binding to Fv ($K_d \sim 0.1$ nM) while reducing affinity for wild-type (WT) FKBP12 by >100-fold ($K_d \sim 250$ nM).[25] This strong allelic preference between mutated Fv and Rim predicts that the use of WT FKBP12 as a binding domain for heterodimer switches, including iRC9, would provide an expected specificity window of about 1,000-fold between iMC and iRC9 after Rim exposure.

To evaluate iRC9 ligand dependency, we measured the efficiency and kinetics of apoptosis in HEK293 cells transfected with plasmids encoding either a truncated caspase-9 with no ligand-binding domain (negative control; C9), Rim-inducible caspase-9 (positive control; iC9), or Rap-inducible caspase-9 (iRC9) (schematic in Figure S1). As a surrogate measure of efficiency of dimerization-dependent apoptosis, a constitutive reporter plasmid, simian virus 40 early promoter and the R-U5 segment of human T cell leukemia virus type 1 long terminal repeat (SRα)-secreted alkaline phosphatase (SeAP) was cotransfected. Reduction of SeAP activity after 18 h of treatment with increasing concentrations of Rim or Rap permitted an estimation of caspase-9 dimerization and induced cell death for each switch (Figure 1B). The iC9 switch was slightly more sensitive to sub-nanomolar ligand relative to Rap-induced iRC9 (EC_{50} = 0.016 nM [Rim] versus 0.35 nM [Rap]). Kinetics and efficacy of each switch was measured by real-time monitoring of caspase-3 and -7 activation via a fluorescent caspase target peptide. iRC9 and iC9 appeared to induce apoptosis with similar kinetics (less than 10 h to full activation) and threshold (Figure 1C). Furthermore, iRC9 was highly active *in vitro* even at 100 pM Rap, with residual activity at even lower drug levels, albeit with slower kinetics. While the therapeutic index is about 3 orders of magnitude, Rim levels above the K_d for WT FKBP12 (i.e., 245–500 nM) began to cross-activate iRC9, as expected.[25] In contrast, even at 1 μM Rap, iC9 was completely ligand insensitive. Similar drug-protein specificity and efficacy were observed in a binary switch when FKBP12-C9 was heterodimerized with FRB-C9 by Rap in HEK293 cells and in primary human T cells (Figure S2).

The selectivity of iRC9 for Rap and iC9 for Rim *in vitro* was predicted by the known ligand-binding affinities, but the efficacy of each switch *in vivo* is also subject to the pharmacokinetics (PKs) of each drug. To assess iRC9 functionality in an *in vivo* whole-animal model, activated human T cells were co-transduced with a γ-retrovirus encoding a *GFP-firefly luciferase* fusion gene (EGFPFluc) and either iC9 or iRC9. Gene-modified T cells were subsequently injected intravenously (i.v.) into immunodeficient NOD.Cg-Prkdcscid Il2rgtm1Wjl/SzJ (NSG) mice.[42] The following day (0 h), mice were treated with Rim (5 mg/kg), Rap (10 mg/kg), or vehicle alone (Veh), and bioluminescence imaging (BLI) was performed to monitor live T cells (Figure 1D). iC9- and iRC9-modified T cells were selectively ablated by Rim and Rap, respectively ($p = 0.018$ and $p = 0.0006$, one-way ANOVA) (Figures 1D and 1E). Importantly, these results also indicate that iRC9 is Rim insensitive at this dose. To confirm BLI measurements, splenocytes were isolated at 24 h post-drug administration and analyzed by flow cytometry. For both iC9- and iRC9-expressing T cells, we observed greater than 80% T cell depletion following Rim or Rap treatment, respectively (Figure 1F). Finally, to determine whether iRC9 is titratable, like iC9,[31] we performed a similar animal experiment using log dilutions of Rap (Figures 1G and 1H). Elimination of iRC9-expressing T cells was titrated with varying Rap doses, allowing a partial reduction of T cell

control iC9 or iRC9-encoding γ-retroviral (RV) vectors. Mice were injected i.v. with 1×10^7 T cells 24 h prior to Rim (5 mg/kg) or Rap (10 mg/kg) treatment i.p. Bioluminescence imaging (BLI) of cells was assessed at −24, 0, 5, and 24 h post-drug administration. (E) BLI of cells at 24 h post-drug administration. (F) Spleens from mice displayed in (D) were collected post-euthanasia for flow cytometry analysis with antibodies to human hCD3, hCD19, and murine mCD45 (as an exclusion marker). **$p < 0.005$, one-way ANOVA. (G) BLI of mice implanted with 1×10^7 GFPFluc and iRC9-expressing human PBMCs 24 h after treatment with Rap at serial 10-fold decreasing dosages. (H) Flow cytometry analysis of CAR-T levels in spleens from mice in (G) harvested 24 h after Rap treatment.

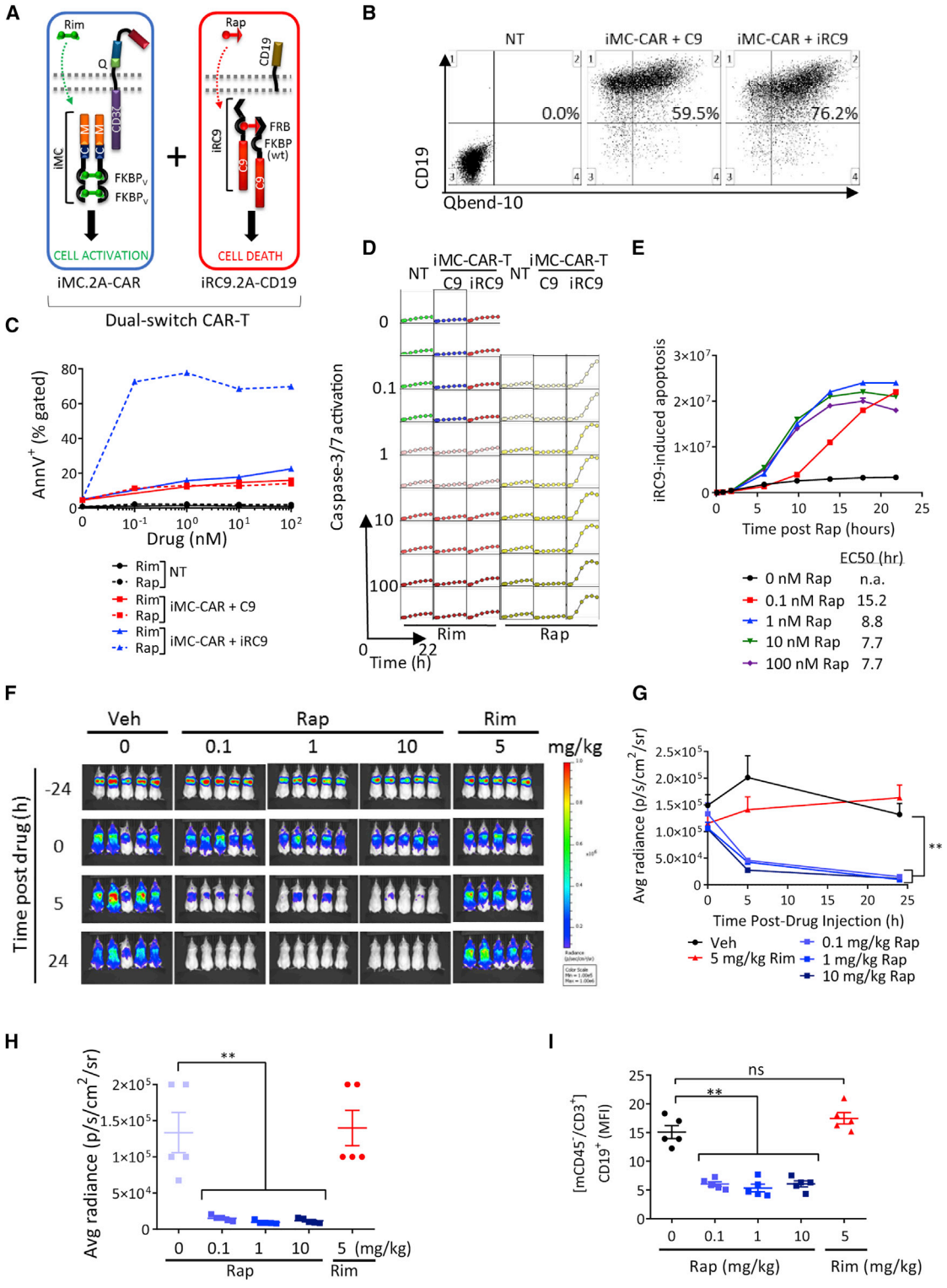

Figure 2. Dose-Dependent Elimination of CD123 CAR-T Cells by iRC9 Activation

(A) Schematic representation of signaling components in dual-switch (DS) CAR-T cells. (B) Activated PBMCs were co-transduced with iMC-CAR and iRC9 (or control C9) γ-RV vectors to produce DS CAR-T cells. NT T cells served as controls. Representative flow cytometry of CD3-gated, CD34$^+$ cells is displayed in which CD19

(legend continued on next page)

frequency (EC_{50} = 0.3 mg/kg).[31] These data indicate that a functional, Rap-activated heterodimeric switch can induce titratable apoptosis at similar levels to that of the conventional homodimerizer-activated iC9 transgene, without appreciable crosstalk.

iRC9 Activation Eliminates Anti-CD123 DS CAR-T Cells in a Dose-Dependent Manner

To determine whether full functionality of iRC9 and iMC is preserved when co-expressed, T cells were co-transduced with iMC-CD123.ζ and iRC9-ΔCD19 γ-retroviruses to generate DS CAR-T cells (Figures 2A and 2B). To maximize iRC9 utility and, hence, safety, DS CAR-T cells co-expressing a signaling-deficient CD19-based surface marker were selected for iRC9-transduced T cells using anti-CD19 microbeads, resulting in more than 95% $CD19^+$ cells, of which the majority co-expressed both vectors. 24-h treatment of control cells (non-transduced [NT] or iMC-CAR-T cells co-expressing caspase-9 [C9]) with up to 100 nM dimerizer (Rim or Rap) revealed no significant apoptosis by flow cytometry (Figure 2C). Conversely, co-expression of iMC-CD123.CAR with iRC9 readily triggered apoptosis with as little as 0.1 nM Rap. Alternatively, cells were exposed to a similar Rap dose range, and caspase-3 and -7 activation was imaged at regular intervals for 22 h as a surrogate indicator for apoptosis (Figure 2D). Interestingly, while there was no difference in maximal cell death levels over 3 logs of Rap, higher ligand concentrations did lead to accelerated apoptosis (Figures 2D and 2E).

To test iRC9 functionality *in vivo* within a DS CAR-T cell platform, EGFPFluc-labeled anti-CD123 DS CAR-T cells were transferred into NSG mice for 24 h followed by a single intraperitoneal (i.p.) dose of 0.1, 1, or 10 mg/kg Rap. As observed in Figure 1, with cells expressing iRC9 only, approximately 80% of CD123-targeted DS CAR-T cells were eliminated within 5 h of Rap treatment, and greater than 90% elimination was evident after 24 h (Figures 2F–2I). In contrast, no significant changes in DS CAR-T cells BLI levels were evident in control mice treated with vehicle alone or 5 mg/kg Rim. Furthermore, flow cytometric analysis of splenocytes showed that $CD19^+$ T cells were essentially eliminated by Rap, but not Rim, treatment ($p < 0.0001$ and $p = 0.44$, respectively) (Figure 2H). These studies indicate that the proapoptotic iRC9 safety switch is rapid and ligand selective, even in the presence of a Rim dose surpassing that required for iMC activation *in vivo*.

While Rim concentration *in vitro* is stable and easy to maintain well below cross-reactive levels to activate iRC9, it was unclear whether a bolus Rim administration *in vivo* might transiently achieve peak (C_{max}) Rim levels sufficient to activate the safety switch. To evaluate this possibility, we increased the Rim dose up to 50-fold above that typically required for iMC activation in NSG mice implanted with DS CAR-T cells. While peak (Rim) in plasma approached 8 μg/mL (Figure S3A), activation of the safety switch as measured by BLI or by vector copy analysis was still not detected (Figures S3B–S3D). These observations strongly support that crosstalk between Rim (at practical levels for iMC activation) and WT FKBP12-containing iRC9 is negligible.

iMC Provides CD123-Specific DS CAR-T Cell Costimulation and Enhances Antitumor Activity

When combined with a first-generation CAR, iMC provides potent inducible CAR-T cell costimulation that augments CAR-T activity in a controllable manner.[17,23] To determine if iRC9 addition to the iMC-CAR platform affected antitumor activity, CD123-targeted DS CAR-T cells were compared directly with iMC-CD123.ζ-modified T cells via a 7-day *in vitro* co-culture assay to measure cytokine production, tumor killing, and CAR-T cell proliferation in the presence or absence of Rim (Figure 3A). After 48 h at a 1:10 effector-to-target (E:T) ratio with $CD123^+$ THP1 acute myeloid leukemia (AML) cells, Rim-induced interleukin-2 (IL-2) production was virtually identical between single-switch iMC-CAR-T cells and DS CAR-T cells (Figure 3B). THP1 cell elimination over a 7-day time course was also Rim enhanced in both single-switch and DS CAR-T cells, showing that iRC9 co-expression does not impair tumor killing (Figure 3C). In addition, CAR-T cell proliferation and cytokine production were Rim titratable (Figures 3D–3F; Figures S4A–S4C). Moreover, iMC activation in either the single-switch or DS formats did not affect CAR specificity, as $CD123^-$ human pancreatic cancer (HPAC) tumor cells were resistant to CD123 DS CAR-T cells with or without Rim (Figure S4D). Similarly, control HER2-specific DS CAR-T cells did not produce cytokines or demonstrate cytotoxicity against $Her2^-$ $CD123^+$ THP1 or MOLM13 cell lines, unlike the CD123-specific DS CAR-T cells, which exhibited dose-dependent cytokine release, tumor cell killing, and expansion (Figures 3D–3H; Figures S4B, S4C, and S4E).

To further evaluate *in vivo* DS efficacy, we examined the utility of the iMC switch to enhance CD123-specific DS CAR-T cells for control of established THP1 leukemias in NSG mice. Following the infusion of 2.5×10^6 NT or DS CAR-T cells, Rim (1 mg/kg) or placebo was administered the same day and at day 15 post-T cell infusion. In the absence of Rim treatment, CD123 DS CAR-T and NT T cells were unable to control THP1 tumor growth, while Rim stimulation

magnetic-activated cell sorting (MACS) selection resulted in >90% $CD19^+$ purity. (C) 24 h post-drug treatment, T cells from (B) were annexin V and propidium iodide stained and analyzed for apoptosis by flow cytometry. (D) T cells were seeded with increasing Rim or Rap in the presence of caspase-3 and -7 substrate (2 μM) to monitor caspase activity in real time in an IncuCyte chamber. (E) Graphical comparison of the speed of iRC9-induced T cell apoptosis with increased Rap dose. Data extracted from (D). (F and G) NSG mice were implanted i.v. with 1×10^7 CD19-selected T cells 24 h before i.p. treatment with Rim (5 mg/kg) or Rap (0.1, 1, and 10 mg/kg). (F) IVIS images were taken at −24, 0, 5, and 24 h post-drug administration and (G) BLI quantitated and graphed over time. BLI of cells was assessed at −24, 0, 5, and 24 h post-drug administration. (H) BLI of cells at 24 h post-drug administration. (I) Spleens were collected post-euthanasia for flow cytometry analysis of transduced cells with antibodies to hCD3, hCD19, and mCD45. Geometric mean fluorescence intensity (MFI) is plotted. **n = 5; $p < 0.005$, one-way ANOVA.

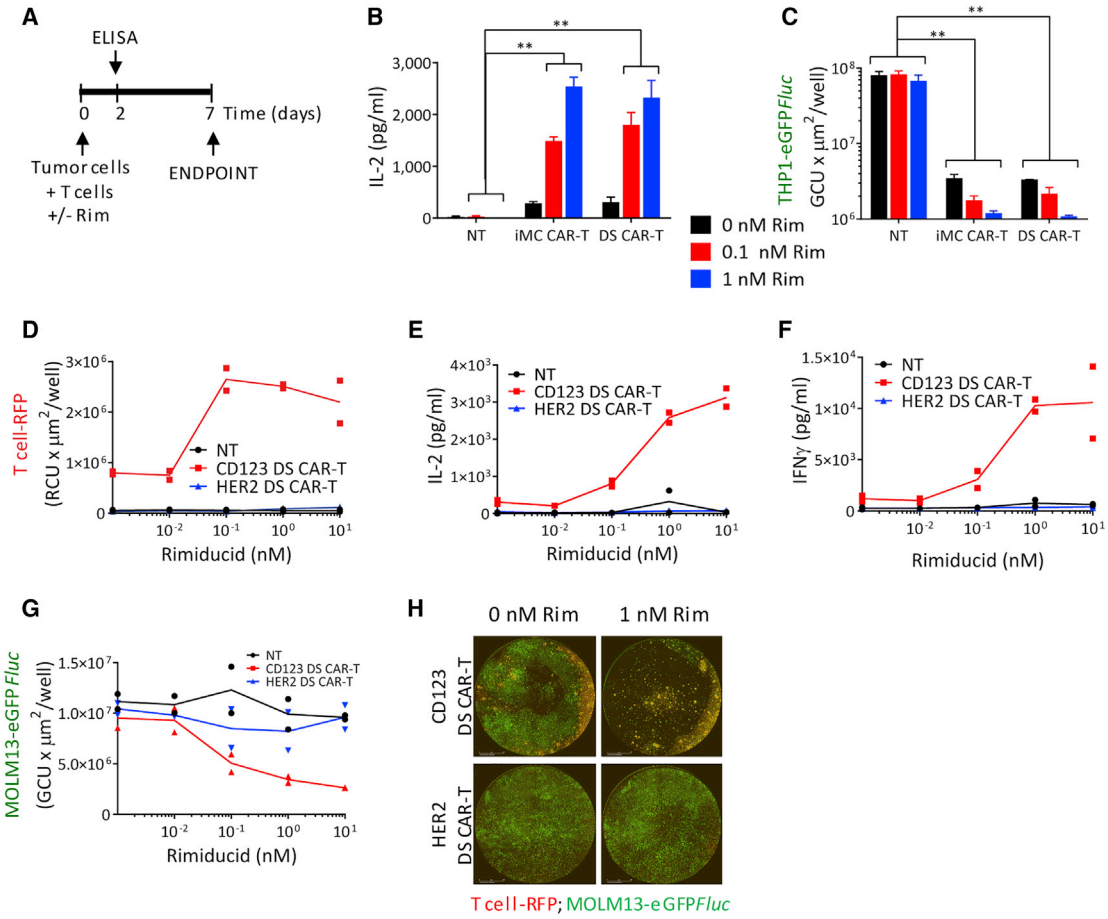

Figure 3. Rimiducid-Mediated iMC Activation Enhances *In Vitro* Killing of CD123⁺ AML Cells by CD123 DS CAR-T Cells

(A) NT, iMC-CAR, and DS CAR-T cells were co-cultured with CD123⁺ THP1-GFP tumor cells at a 1:10 effector-to-target (E:T) ratio and treated with 0, 0.1, and 1 nM Rim. (B) At 2 days post-seeding, culture supernatants from a duplicate plate were analyzed by ELISA for IL-2 production. (C) THP1-GFP tumor growth was monitored in real time in an IncuCyte chamber and analyzed for green fluorescence intensity (GCU × µm²/well) on day 7. (D–H) NT, CD123, or HER2 DS CAR-T cells were co-cultured with CD123⁺ MOLM13-GFP cells with increasing Rim. (D) T cells were co-labeled with red fluorescent protein (RFP) to track T cell expansion via red fluorescent intensity (RCU × µm²/well) as a function of Rim dose. (E and F) 2 days post-seeding, culture supernatants from a duplicate plate were analyzed by ELISA for (E) IL-2 and (F) IFN-γ production. (G) Molm13 tumor growth was monitored in real time and analyzed for green fluorescent intensity (GCU × µm²/well) on day 7. (H) Representative images of co-cultures containing MOLM13-GFP and RFP-labeled CD123 or HER2 DS CAR-T cells on day 7 in the presence or absence of Rim.

greatly enhanced tumor control (Figure 4A). After 30 days, a vector copy number (VCN) assay on freshly isolated splenocytes demonstrated Rim-promoted iMC-enabled DS CAR-T cell expansion (Figure 4B). Together, these *in vitro* and *in vivo* assays clearly indicate that iRC9 addition to iMC-encoding CAR-T cells does not negatively impact iMC-dependent activity (e.g., cytokine production, tumor killing, and CAR-T cell proliferation).

Switching DS CAR-T Cells on and off

Rap (sirolimus) and analogs like temsirolimus (Tem) are FDA-approved immunosuppressants and anti-cancer agents that normally function via mTOR (TORC1) inhibition; however, in the context of the iRC9 safety switch, these drugs have been repurposed as dimerizers to induce apoptosis. To determine whether iMC-mediated proliferative and/or pro-survival signals interfere with iRC9 function or vice versa, we investigated the outcome of Tem treatment *in vivo* on iMC-activated CD123-specific CAR-T cells co-expressing either iRC9 or control caspase-9 (C9) (Figure 4C). Two weekly Rim (1 mg/kg) treatments promoted CAR-T cell expansion, which was followed by a single Tem dose at day 15 to reverse expansion and reduce CAR-T cell numbers. The degree of DS CAR-T cell ablation was Tem-dose dependent over a 100-fold window (Figures 4C and 4D). The expected reduction of gene expression and cell proliferation of a 1 mg/kg Tem dose in control C9-expressing cells was reflected by a 3-fold reduction of CAR-T cell BLI, while iRC9 activation at the same dose reduced CAR-T numbers over 12-fold. The Tem dose-dependent reduction of DS CAR-T cell BLI was also reflected by an even larger reduction in cytokine levels 24 h after activation of the

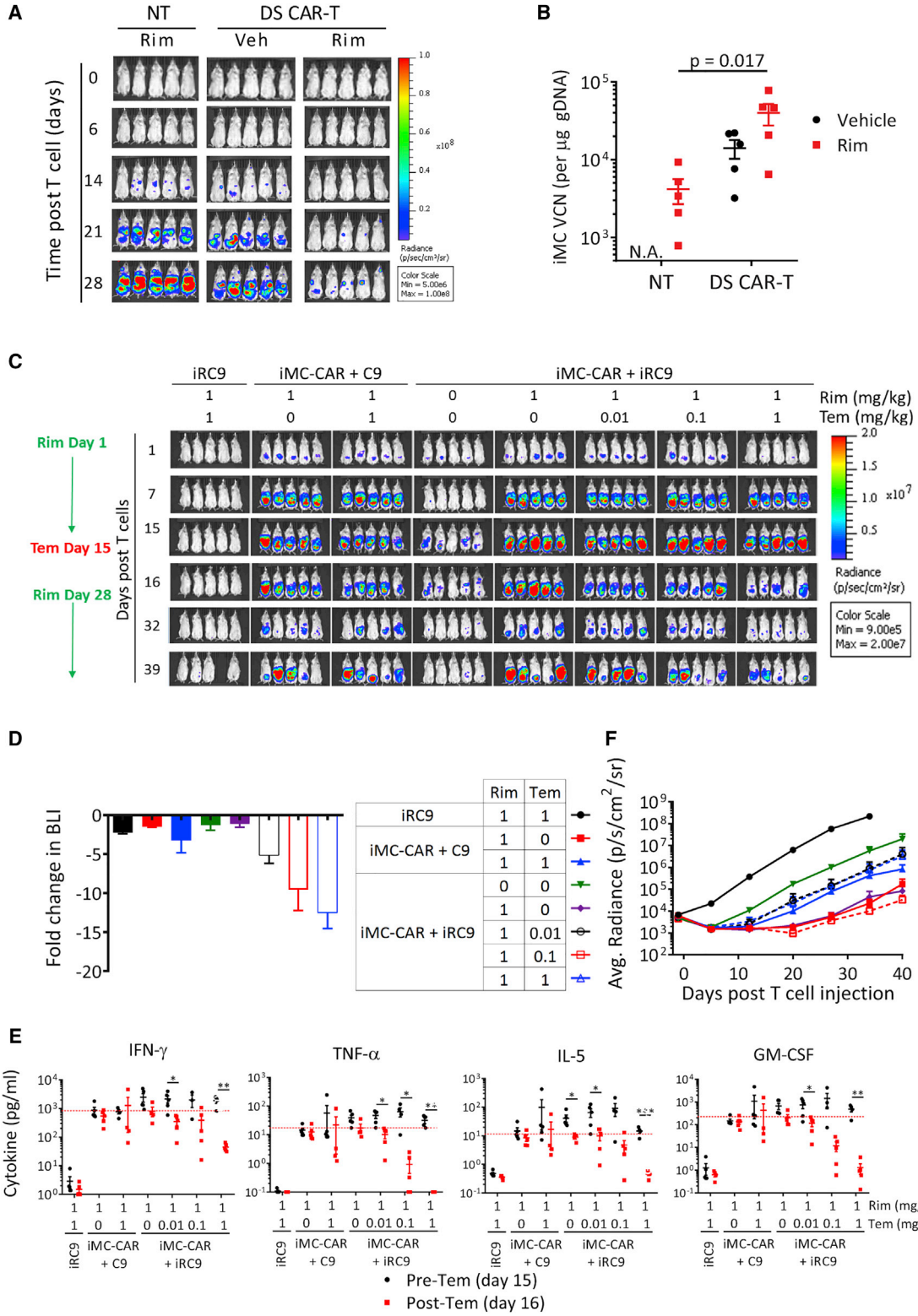

(legend on next page)

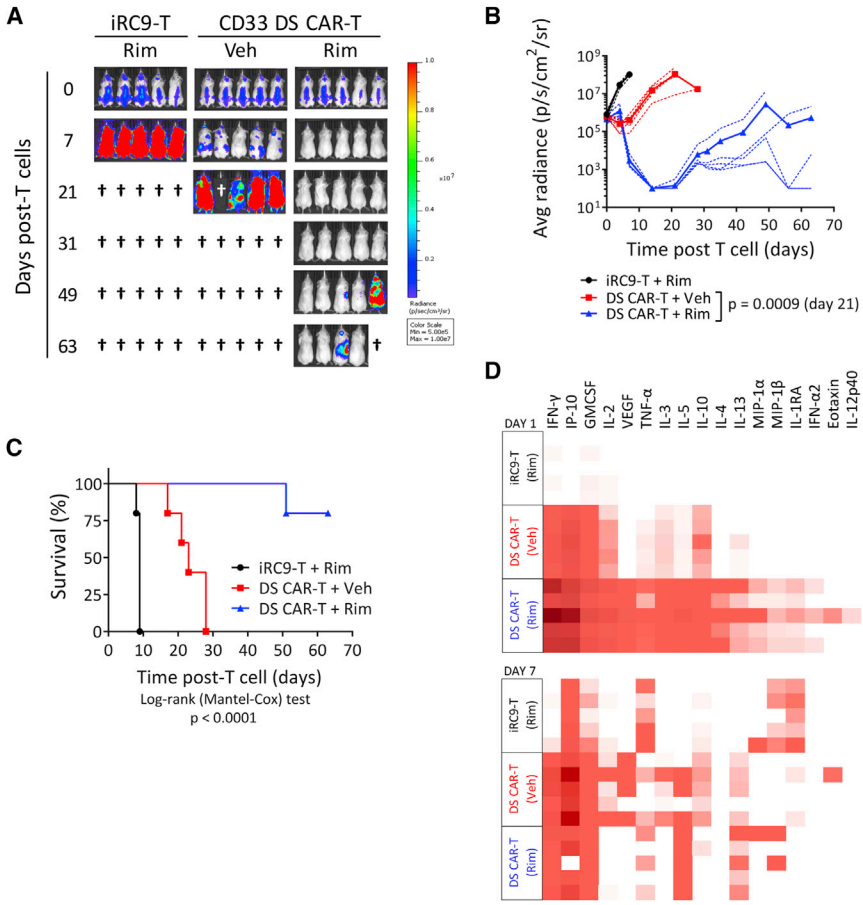

Figure 5. Rimiducid-Mediated iMC Activation Is Required for CD33 DS CAR-T Cells to Control AML *In Vivo*

(A) NSG mice were engrafted i.v. with 5 × 10^5 MOLM13-EGFPFluc cells for 6 days followed by i.v. infusion of 5 × 10^6 CD33 DS CAR-T cells. Rim (1 mg/kg) or placebo was given i.p. starting on the same day as T cell injection and weekly thereafter. MOLM13-EGFPFluc growth was monitored via BLI by IVIS. (B) Individual mice are plotted with dotted lines and averaged groups are plotted in bold. Multiple t test. (C) Kaplan-Meier analysis of mice up to day 63 after T cell injection. Mice in the negative control iRC9 group were sacrificed within 9 days after T cell treatment due to large tumor burden. The CD33 DS CAR-T + Rim group demonstrated the optimum survival benefit, although one of five mice needed to be euthanized at day 51 due to tumor recurrence. (D) Human cytokine multiplex analysis of serum samples collected from a second experiment with the same design on days 1 and 7 after T cell and Rim treatment.

safety switch (Figure 4E). Further, we determined if remaining DS CAR-T cells surviving 13 days following iRC9 activation retain some useful functionality. Interestingly, reactivation (with Rim) of the surviving DS CAR-T cells after relatively low Tem dose demonstrated that this residual pool of DS CAR-T cells can re-expand (Figure 4C) to maintain tumor control, if needed (Figure 4F). This underscores a useful feature of the DS system when only a portion of highly activated therapeutic T cells need to be eliminated to control toxicity.

To study the general applicability of the DS platform toward multiple antigens, distinct DS iMC-enabled, CD33-targeted CAR-T cells were tested against the aggressive $CD33^+$ AML tumor line, MOLM13. NSG mice were engrafted with MOLM13-EGFPFluc tumor cells for 6 days, followed by the injection of iRC9-only T cells or CD33 DS CAR-T cells. Rim or placebo was administered starting on the same day as T cell injection and weekly thereafter. Tumor control by CD33 DS CAR-T cells was apparent as early as day 7 after T cell administration, but Rim-mediated iMC stimulation was necessary for durable tumor control, as the vehicle-treated DS CAR-T cell group succumbed to tumor outgrowth starting at day 20 (Figures 5A–5C). In a parallel experiment, we measured serum cytokine levels collected at days 1 and 7 following T cell and Rim treatment (Figure 5D). This showed that Rim treatment of CD33 DS CAR-T cells transiently induced high levels of cytokines and chemokines that are associated with T cell activation and inflammation (interferon [IFN]γ, granulocyte-macrophage colony-stimulating factor [GM-CSF], and interferon gamma-induced protein 10 [IP-10]), proliferation (IL-2), and antitumor activity (tumor necrosis factor alpha [TNF-α]), which generally

Figure 4. Rimiducid-Mediated iMC Activation Is Required for AML Tumor Cell Killing *In Vivo*

(A) NSG mice were engrafted with 1 × 10^6 THP1-GFPFluc cells i.v. for 7 days followed by i.v. infusion of 2.5 × 10^6 T cells. Rim (1 mg/kg) or placebo was administered i.p. on days 0 and 15 post-T cell infusion. THP1-EGFPFluc growth was monitored by *in vivo* imaging system (IVIS). (B) On day 30, mice were sacrificed, and spleens were analyzed for the presence of CAR-T cells (iMC and iRC9 gDNA levels) using a PCR-based vector copy number (VCN) assay. (C) Activation of the "Go" and "Stop" switches. NSG mice were engrafted with 1 × 10^6 THP1-EGFPFluc cells i.v. for 7 days followed by infusion of 5 × 10^6 CD123 DS CAR-T cells (i.v.). CAR-T cells were marked with Orange Nanolantern *Renilla luciferase* (ONLRluc). Rim (1 mg/kg) or placebo was given i.p. on days 1 and 8. Temsirolimus (0 to 1 mg/kg) was administered on day 15 when some mice began to display cytokine release syndrome (CRS) symptoms (e.g., weight loss, ruffled fur). CD123 DS CAR-ONLRluc expansion was measured by IVIS using BLI and coelenterazine substrate. Rimiducid (5 mg/kg) was re-administered at days 28, 32, 35, and 38 to expand remaining DS CAR-T cells. (D) Relative fold change in T cell BLI following Tem treatment from day 15 to day 16 in the experiment described in (C). (E) Blood was collected pre- and 24 h post-Tem treatment for Multiplex analysis of cytokines present in serum. *p < 0.05, **p < 0.005, ***p < 0.0005, multiple t test. (F) Growth of THP1 tumors in the mice described in (C) measured by BLI from D-luciferin substrate. Legend is to the left.

reverted to control (vehicle) levels within one week of drug treatment. Together, these results indicate that this DS technology is broadly applicable to multiple leukemic targets.

Activation of DS CAR-T Cells against Solid Tumors

To evaluate the DS CAR-T cell platform in additional tumor settings, we generated HER2-specific DS CAR-T cells to target $HER2^+$ solid cancers. As with CD123-specific DS CAR-T cells, iMC activation with low Rim doses stimulated robust production and release of IL-2 to support CAR-T cell proliferation and killing of $HER2^+$ HPAC tumor cells, even at low E:T ratios (i.e., 1:80 CAR-T to HPAC) in a 7-day co-culture assay (Figures S5A–S5C). Representative fluorescent images captured at day 7 of co-culture with HPAC-RFP target cells at a low 1:40 E:T ratio showed that 1 nM Rim greatly improved tumor cell killing and T cell expansion (Figure S5D). This supports that, even against solid tumor lines, there is sufficient iMC expression in the DS platform to augment tumor control *in vitro*.

To determine whether the DS platform could perform comparably to iMC-CAR-T cells against solid tumors *in vivo*, we attempted to normalize gene expression by magnetic-activated cell sorting (MACS) selection for either the CD19 marker (iRC9 control or HER2 DS cells) or the CAR-embedded CD34 Q-Bend-10 epitope (iMC-CAR-T cells only). Although the DS CAR-T cells were only selected for the safety switch, following enrichment, 80% of the population also co-expressed the CAR and iMC encoded by the co-transduced virus (Figure S6A). Western blot analysis indicated that, although the iMC level of DS CAR-T cells was somewhat lower than that of single-switch-expressing iMC-CAR-T cells, it was increased following selection (Figure S6B). Moreover, iRC9 protein levels of dually transduced DS CAR-T cells were lower than those of iRC9-only T cells, but they were also enriched following selection. Therefore, based on ample protein expression of DS platform components, DS protein expression would be expected to perform similarly to CAR-T cells expressing iMC alone.[17]

Finally, HER2 DS CAR-T cells demonstrated effective antitumor activity against OE19 esophageal tumors implanted subcutaneously into NSG mice, which was further enhanced by Rim ($p = 0.004$) (Figure S6C). *In vivo* BLI monitoring of T cell expansion also showed enhanced Rim-dependent T cell proliferation in DS CAR-T cells (Figure S6D). Interestingly, the one tumor (of 5) that escaped Rim-stimulated HER2 DS CAR-T cell treatment at 5 weeks had greatly reduced levels of the CAR-specific antigen (Figure S6E). In a follow-up experiment using a lower CAR-T cell dose but with more frequent Rim dosage, consistent Rim-dependent tumor control (Figures 6A and 6C–6E) and DS CAR-T cell expansion were observed (Figures 6B and 6F) that persisted for weeks following tumor control. Cytokine expression at day 19 (when tumor was mostly eradicated) largely correlated with the expansion of DS CAR-T cells in drug-treated mice (Figure 6G), and the profile of cytokines was similar to that of CD33 DS CAR-T cells at day 1 (Figure 5D), with the exception of vascular endothelial growth factor (VEGF), IL-4, and IL-2, which are likely to require multiple signals from iMC and Rim and continuous CAR engagement. Together, these results demonstrate that, in the context of the DS CAR platform, iMC activation provides sufficient costimulation to CAR-T cells to home to and eliminate solid tumors *in vivo*.

DISCUSSION

Unlike small molecules with well-defined pharmacokinetics, the unpredictability of cellular therapies creates unique treatment challenges, particularly with regard to dose control. The ability to better regulate the activity and survival of these living drugs has the dual benefit of promoting efficacy without abandoning safety. Notably, each of the dimerizing ligands tested here, Rap, Tem, and Rim, have sufficient pharmacokinetic and pharmacodynamic profiles to activate iRC9 and iMC *in vivo*, supporting their clinical utility. The iMC and iRC9 switches are each functionally inducible at sub-nanomolar ligand concentrations, and they reflect orthogonality due to the allele specificity of mutant FKBP12V36 toward Rim. This feature supports a therapeutic window in excess of 100-fold (i.e., iMC is activated by 1 nM Rim while iRC9 requires greater than 100 nM Rim to trigger cell death). While peak Rim levels measured during infusion to activate iMC costimulation *in vivo* could theoretically activate the safety switch,[43] treatment of DS CAR-T cell-bearing NSG with a grossly excessive dose (50-fold above that required for standard iMC activation) failed to activate the safety switch, despite a C_{max} approaching 8 μg/mL (~ 5.6 μM). High serum protein-binding affinity of Rim (i.e., >99.9% of Rim in plasma is mostly albumin bound) likely prevents peak free drug levels from surpassing the 250-nM binding affinity for WT FKBP within iRC9. Together, this strongly supports the orthogonal use of Rap (or analogs) with Rim *in vivo* in a DS platform for CAR-T cell costimulation and apoptosis.

Cell dose control remains a critical element in the maturation of cell therapy. We have shown that Rim-activated DS CAR-T cells can effectively kill both liquid and solid tumors while concomitantly retaining the capacity for efficient Rap-mediated T cell elimination if acute toxicity were to occur. For some highly malignant indications, such as CD33- or CD123-targeted AML, high levels of costimulatory activity may be required over a brief period for maximum CAR-T cell efficacy. Because these antigens are also expressed in hematopoietic stem and myeloid precursor cells, effective elimination of the therapeutic cells will be necessary following the reduction of tumor burden to limit on-target but off-tumor toxicities, like neutropenia, and to protect against severe cytokine release syndrome (CRS) in patients with high tumor burden. Use of iRC9 to reduce or even eliminate auto-reactive CAR-T cells after the achievement of minimal residual disease negative (MRD^-) status could provide an adjunct to conditioning that precedes an invasive allogeneic bone marrow transplant, or it could even obviate the need for transplantation altogether in some cases.

The addition of costimulatory molecules (e.g., CD28 and 4-1BB) to first-generation CAR-T cells led to greater CAR-T cell expansion and persistence, underlying the transformational change that CD19-CAR-T cells have had on the management of B cell malignancies. Although success in solid tumors has lagged, in part due to the relative inaccessibility of tumors and the inhibitory tumor

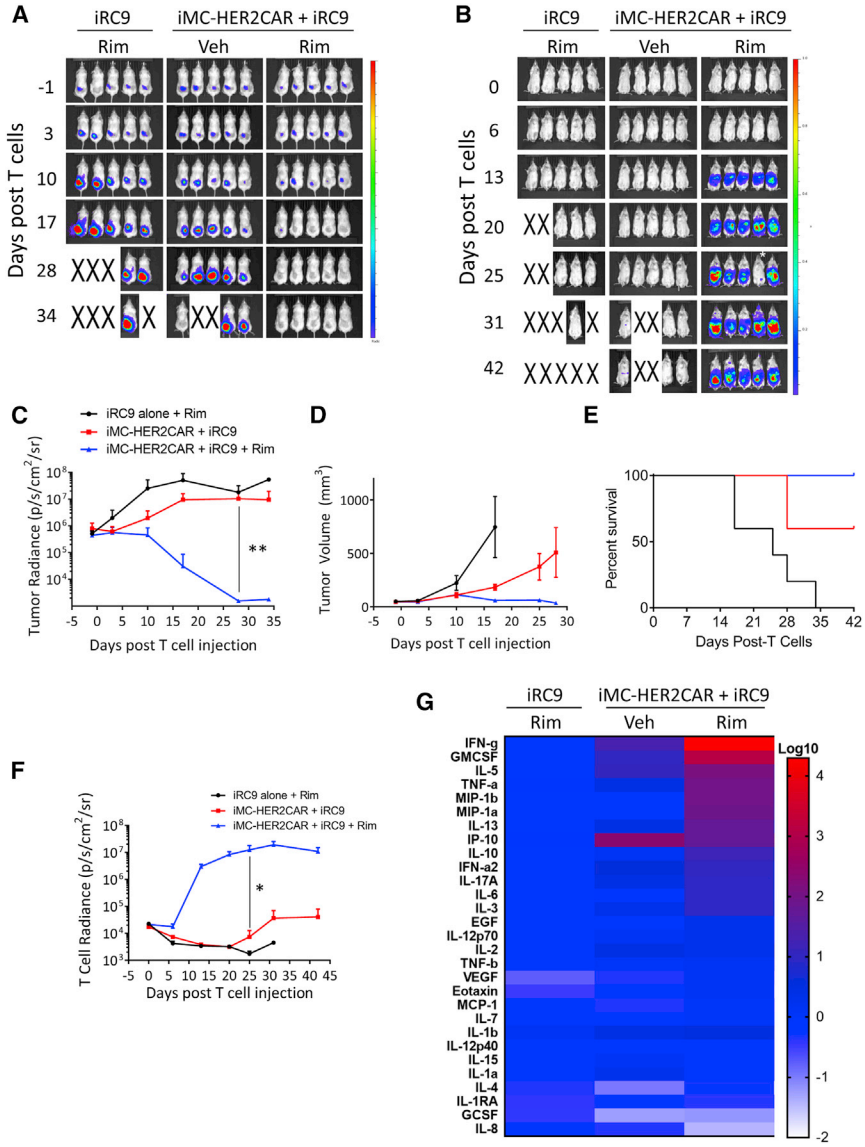

Figure 6. Activation of iMC Enhances DS CAR-T Cell Expansion and HER2⁺ Solid Tumor Killing

2×10^6 OE19-EGFPfluc cells were implanted subcutaneously into NSG mice. 5×10^6 T cells transduced with iRC9-ΔCD19 vectors with or without HER2-targeted iMC-CAR vector, selected for ΔCD19 expression and labeled with ONLRluc, were engrafted i.v. 4 days later (day 0). Rim (1 mg/kg) or vehicle only was administered 5 times weekly. (A) Tumor expansion was visualized weekly by IVIS BLI with D-luciferin as a substrate. The color scales for (A) and (B) indicate $1 \times 10^6 - 1 \times 10^8$ p/s/cm²/sr. (B) Rim-dependent CAR-T cell expansion was visualized weekly. *A mouse was misinjected with coelenterazine substrate on day 25 and this point was not included in data analysis. (C) Quantitation of tumor BLI. **p = 0.0388, unpaired t test. (D) Tumor volume over time was measured with calipers. (E) Kaplan-Meier analysis of mouse survival over 6 weeks. Endpoints were achieved at a tumor area of 150 mm². p = 0.026, log-rank test, Mantel-Cox test. (F) Quantitation of T cell expansion. *p = 0.043 unpaired t test. (G) Multiplex analysis of serum cytokine levels at day 19 relative to the mean of the iRC9-only group on an exponential scale.

microenvironment encountered upon arrival within antigen-expressing tumors, there does appear to be some evidence of a correlation between CAR-T cell persistence (generally measured clinically by indirect observation of the peripheral blood) and efficacy against solid tumors.[44–47] Interestingly, in a study of EGFRvIII-specific CAR-T cells in recurrent glioblastoma patients, O'Rourke and colleagues reported data that suggest a correlative window between CAR-T cell expansion in peripheral blood and tumor trafficking.[44] As iMC signaling can also impart onto CAR-T cells potent proliferative and pro-survival advantages,[17,23] and it can be Rim-tuned to gradually increase or aggressively enhance CAR-T cell expansion as required by the tumor level or type, it is likely to be useful to maintain CAR-T cell survival for long-term surveillance against disease relapse. Furthermore, the constellation of cytokines and chemokines whose secretion can be governed by iMC activation, including IFNγ, GM-CSF, IP-10, CCL2, and CCL3, are likely to increase antigen expression on tumor cells and promote the recruitment and activation of monocytes, dendritic cells, and lymphocytes in a pro-inflammatory antitumor response that may also mitigate a hostile anti-immune tumor microenvironment and re-ignite the endogenous immune response. This potentially differentiated adjuvant feature of iMC is made more exploitable by the inclusion of a rapid and efficient safety mechanism, iRC9, to rapidly attenuate excessive cytokine release or off-tumor targeting of healthy tissues with low-level target expression.

As observed for clinically validated iC9,[27,48] the variant safety switch iRC9 is not simply an on-off switch with the capacity to eliminate therapeutic T cells, but it reflects dose-dependent sensitivity. In cases of toxicity from excessive cytokine release, low Rap concentrations (i.e., ~0.1 mg/kg in mice) are likely sufficient to attenuate CAR-T function while preserving the capacity for re-expansion of surviving DS CAR-T cells to respond to residual tumor. As clinical CAR-T and recombinant TCR approaches expand to new target antigens, off-tumor targeting will likely be seen more frequently, as toxicity screens based on cells, tissue, and animal models (often lacking immunoreactive target antigen) may prove insufficient to detect all off-tumor risks. In preclinical models, the administration of high doses of Rap resulted in the ablation of a large portion of CAR-T cells (>90%), which may translate into reduced risk of severe off-target toxicities; however, at present, the most effective risk mitigation for off-target toxicities is through the selection of highly specific tumor-antigen targets (e.g., EGFRvIII), something

that has proven challenging in solid tumors, illustrating the importance of continued research in the field of antigen discovery and tumor biology.[49] The speed of the iRC9 proapoptotic switch relying on small molecules with clinically desirable pharmacological characteristics may be a key feature of its ability to reduce toxic cytokine levels (Figure 4), although further experimentation in cross-reactive animal models will be needed to demonstrate the mitigation of acute CAR-T cell targeting of essential organs. Other safety switches have been developed to control the toxicity of CAR-T cell therapy, such as the use of marker proteins engaged by clinically available antibody-dependent cellular cytotoxicity (ADCC) engagers (e.g., anti-CD20).[50–52] However, due to complement activation that can also occur, such strategies would be inherently pro-inflammatory and may even exacerbate acute toxicity, but they are likely suitable for less acute off-tumor targeting, such as the attenuation of B cell aplasia by CD19 CAR-T cell therapy and stem cell depletion from CD123-targeted CAR-T cells,[52] where removal of most or all marker-expressing CAR-T cells over days is beneficial.

Several dimerizer technologies have been described since the first description of chemically induced dimerization (CID) using a synthetic FK506 homodimerizer, but only a handful is based on syngeneic (and hence non-immunogenic) ligand-binding proteins required for long-term expression in an immunocompetent host. FKBP12 and FRB domains are each human derived, and both Rim and Rap are clinically available and relatively easy to administer to patients. Tandem fusion of FKBP12 with FRB provides a simple, potentially versatile mechanism to utilize Rap, a clinically approved pharmaceutical, as an agent to homodimerize and activate signaling domains even though Rap is mechanistically a FRB-FKBP heterodimerizer. Although signaling domains would appear offset when dimerized or oligomerized in this fashion, this work demonstrates that it is clearly possible to achieve enough flexibility between protein domains in iRC9 for fully functional dimerization and activation. For the iRC9 proapoptotic safety switch or recently described analogous Rap-regulated caspases,[53] the potential transient side effect of TORC1 inhibition by Rap is irrelevant to CAR-T cells marked for removal, and it could even contribute to tumor control. In contrast, for activation switches based on FRB-FKBP fusions, a non-immunosuppressive Rap derivative would likely be required for most applications.[38,40,54] Taken together, these data provide the groundwork for building clinically applicable CAR and TCR products with two dimensions of regulation covering both cell activation and attenuation. While this work focused on the control of T cell therapy, the DS technology described herein for the first time should also have extremely broad biomedical applications in the context of similar or disparate signaling pathways.

MATERIALS AND METHODS

Cell Lines, Media, and Reagents

HEK293T, HEK293, THP1, HPAC, OE19 (all from ATCC, Manassas, VA), and MOLM-13 (DSMZ, Braunschweig, Germany) were cultured in media per the suppliers' recommendations. Clinical-grade Rim was diluted in ethanol, as a 100-μM working solution for *in vitro* assays, and further into 0.9% saline for animal studies. Research-grade Rap (LC Laboratories) and Tem (Sigma) were dissolved in ethanol, as a 100-μM working solution for *in vitro* assays, and in Injection Diluent (10% polyethylene glycol [PEG]-400 + 5% Tween-80) for animal studies.

Retroviral and Plasmid Constructs

The iMC-CAR-T vector has been previously described.[17] Various single-chain variable fragments (CD123 = 32,716 single-chain variable fragments [scFvs], CD33 = My9.6 scFv, and HER2 = 4D5-8 scFv) were cloned via enzymatic digestion to swap for different antigen-specific iMC-CAR-T cells. Synthetic DNA (Integrated DNA Technologies, San Diego, CA) encoding the truncated caspase-9 gene only (C9), $FKBP_V$ fused in-frame to caspase-9 (iC9), and tandem FRB and FKBP12 domains fused in-frame to caspase-9 (iRC9) were cloned into the same plasmid backbone (pSFG) retroviral backbone (Figure S1). These vectors also contain a truncated CD19 (ΔCD19) separated by a *Thosea asigna virus* 2A (T2A) peptide bond-skipping polypeptide. Tumor cells and T cells were transduced with the pSFG-EGFP-*Firefly luciferase* (EGFPFluc), pSFG-orange Nano-lantern *Renilla luciferase* (ONLRluc), or pSFG-nuclearRFP retroviruses.

Activation and Transduction of T Cells

Peripheral blood mononuclear cells (PBMCs) were isolated from buffy coats obtained through the Gulf Coast Regional Blood Center, and they were cultured in 45% RPMI 1640 and 45% Click's media (Invitrogen, Grand Island, NY), supplemented with 10% fetal bovine serum (FBS) and 100 U/ml IL-2 (Miltenyi Biotec). Buffy coats were tested negative for infectious viral pathogens. Retrovirus was produced by transient transfection of HEK293T cells using GeneJuice (EMD Millipore, Billerca, MA) with MoMLV gag-pol (PegPam3-e plasmid), RD114 envelope (RDF plasmid), and the pSFG retroviral vector encoding the transgenes. Supernatant was collected after 48–72 h to transduce T cells that were activated by stimulation with 0.5 μg/mL each of anti-CD3 and anti-CD28 antibodies (Miltenyi Biotec) in the presence of 100 U/mL IL-2. The spinfection technique was performed to transduce T cells with RetroNectin coating and expanded for 10–14 days post-transduction unless otherwise stated. For transductions with multiple vectors, the protocol was identical to the above, except the wells were coated with equal amounts of each retroviral supernatant.

Phenotyping and *Ex Vivo* Cell Counting

Transduction efficiency was determined by flow cytometry using anti-hCD3 BV510 (BioLegend), anti-hCD19 BV421 (BioLegend), and anti-hCD34 phycoerythrin (PE) (Abnova) or anti-CD34 allophycocyanin (APC) (R&D Systems) antibodies. To examine the phenotype of T cells in mice, spleens were isolated, and single-cell suspensions were made by lysing red cells with ammonia chloride-potassium (ACK)-based lysis buffer, followed by mechanical dissociation through a 70-μm nylon filter. Cells were subsequently stained with the following antibodies: anti-hCD3 PerCP Cy5.5, anti-hCD19-APC, anti-hCD34 PE, and anti-mCD45RA BV510. Total transduced T cell numbers in the spleens were calculated by counting

total splenocyte numbers and multiplying by the percentage of $CD3^+$ and $CD19^+$ or $CD3^+$ and $CD34^+$ T cells observed by flow cytometry on a Gallios cytometer (Becton Dickinson).

Cytokine Production

Production of IFN-γ and IL-2 by transduced T cells was analyzed by ELISA (eBioscience, San Diego, CA). Cytokines were also analyzed using a 27-cytokine and chemokine multiplex array system with a multiple reader (MILLIPLEX MAP kit, Luminex reader; EMD Millipore).

SRα-SeAP Assay in 293 Cells

On day 0, 5×10^5 HEK293 cells were seeded onto 6-well plates in 2 mL DMEM (10% FBS + 1% penicillin[pen] and streptomycin [strep]). On day 1, cells were co-transfected with 1 μg each of plasmid expression vectors and the SRα-SeAP reporter plasmid. On day 2, cells were collected, seeded onto 96-well plates containing 2× concentrated half-log drug dilutions, and analyzed by fluorescence-activated cell sorting (FACS) for transfection efficiency. On day 3, the drug-treated cells were heat inactivated at 68°C for 1 h, and supernatants were added to black 96-well plates (Greiner) containing 1 mM 4-methylumbelliferyl phosphate (MUP) substrate (2× concentration) diluted in 2 M diethanolamine. The plates were incubated at 37°C for 30 min or overnight, and fluorescence excited at 355 nm and emitting at 460 nm was measured.

Western Blot Analysis

After transduction with the appropriate retrovirus(es), T cells were collected, washed in cold PBS, and lysed in radioimmunoprecipitation assay buffer (RIPA) Lysis and Extraction Buffer (Thermo Fisher Scientific) containing 1× Halt Protease Inhibitor Cocktail (Thermo Fisher Scientific) on ice for 30 min. The lysates were centrifuged at 16,000 × g for 20 min at 4°C, and supernatants were transferred to new Eppendorf tubes. Protein assay was performed using the Pierce BCA Protein Assay Kit (Thermo Fisher Scientific), per the manufacturer's recommendation. To prepare samples for SDS-PAGE, 50 μg lysates was mixed with 4× Laemmli Sample Buffer (Bio-Rad) and heated at 95°C for 10 min. Meanwhile, 10% SDS gels were prepared using Bio-Rad casting apparatus and 30% Acrylamide and bis Solution (Bio-Rad). Samples were loaded along with Precision Plus Protein Dual Color Standards (Bio-Rad) and electrophoresed in 1× Tris and glycine Running Buffer (Bio-Rad) at 140 V for 90 min. After protein separation, gels were transferred onto polyvinylidene fluoride (PVDF) membranes using the iBlot 2 device (Thermo Fisher Scientific). Membranes were probed with primary and secondary antibodies using the iBind Flex Western Device (Thermo Fisher Scientific), according to the manufacturer's recommendation. Primary antibodies used include β-actin (1:1,000, Thermo Fisher Scientific), caspase-9 (1:400, Thermo Fisher Scientific), and MyD88 (1:200, Santa Cruz Biotechnology). Secondary antibodies used were horseradish peroxidase (HRP)-conjugated goat anti-rabbit or mouse immunoglobulin G (IgG) antibodies (1:500, Thermo Fisher Scientific). Membranes were developed using SuperSignal West Femto Maximum Sensitivity Substrate Kit (Thermo Fisher Scientific, 34096) and imaged using a GelLogic 6000 Pro camera and CareStream MI software (version [v.]5.3.1.16369).

In Vitro Fluorescence-Based Assay Using the IncuCyte

For caspase-3 and -7 activation assay, after transfection or transduction with the appropriate retrovirus, 5×10^4 T cells were seeded per well in a 96-well plate in the presence or absence of drugs (Rim or Rap) in the presence of IL-2. To enable detection of apoptosis using the IncuCyte instrument, 2 μM IncuCyte Kinetic Caspase-3 and -7 Apoptosis reagent (Essen Bioscience) was added to each well to reach a total volume of 200 μL. Plates were centrifuged for 5 min at 400 × *g* and placed inside the IncuCyte (Dual Color Model) to monitor green fluorescence every 2–3 h for a total of 48 h at 10× objective. The "Total Green Object Integrated Intensity" (GCU × μm^2/well) metric was used to quantify caspase activation. Each condition was performed in duplicate, and each well was imaged at 4 distinct locations at 10× objective or the whole well was imaged at 4× objective.

For co-culture assay, EGFP*Fluc* or red fluorescent protein (RFP)-modified tumor cells were seeded onto 96-well plates for 2–4 h, followed by T cell seeding at various E:T ratios with or without Rim. Each plate was set up in duplicate, one plate to monitor with the IncuCyte and one plate for supernatant collection for ELISA on day 2. The Total Green Object Integrated Intensity (GCU × μm^2/well) metric was used to quantify green fluorescence, and the Red Object Count (1/well) metric was used to quantify nuclear red fluorescence. Each condition was performed at least in duplicates, and each well was imaged at 4 distinct locations at 10× objective or the whole well was imaged at 4× objective.

Animal Model

NSG mice were obtained from The Jackson Laboratory (Bar Harbor, ME) and maintained at the Bellicum Pharmaceuticals AAALAC-approved vivarium. These studies were approved by the Bellicum Pharmaceuticals Institutional Animal Care and Use Committee (IACUC) comprising both internal and external reviewers. For T cell killing assays, 8-week-old female NSG mice were injected i.v. with 1×10^7 T cells in 100 μL PBS. Mice were subjected to *in vivo* imaging system (IVIS) imaging ∼4 h after T cell injection (−14 h post-drug administration). The following day, mice were imaged just before drug injection (0 h), then injected i.p. with Veh, Rim diluted in Solutol HS15 and saline, or Rap diluted in injection diluent (5% polyethylene glycol 400 and 5% polyoxyethylene sorbitan monooleate). Mice were imaged again at 5–6 h and 24 h after drug injection. Thereafter, mice were sacrificed, and spleens were removed for FACS analysis.

For tumor challenge assays, 8-week-old female NSG mice were initially injected with tumor cells i.v. (THP1 or MOLM13) or subcutaneously (s.c., OE19), followed by i.v. injection of T cells. Rim or Veh was administered i.p. starting on the same day as T cell injection and continued according to different experimental designs. Mice were imaged weekly for firefly or Renilla luciferase activity using luciferin or coelenterazine substrates, respectively. Weight measurement was

performed twice per week. Endpoint analysis involved FACS and copy number analysis of splenocytes and peripheral blood.

VCN Assay

CAR-T cell biodistribution was determined by isolating tissues from treated mice and performing VCN by qPCR. Genomic DNA (gDNA) was isolated from each tissue specimen (<25 mg) using DNeasy Blood & Tissue Kits (QIAGEN). Taqman PCR primers and fluorescent probe were designed to recognize between MyD88 and CD40 (forward, 5′-GGGCATCACCACACTTGAT-3′; reverse, 5′-GCCTTAT TGGTTGGCTTCTTG-3′; FAM-probe: 5′-FAM/ATATGCCTG/ ZEN/AGCGTTTCGATGCCT-3′). Taqman PCR primers and fluorescent probe were designed to recognize C9 (forward, 5′-GCA GTGGGCTCACTCTGAAGA-3′; reverse, 5′-CCCTTTCACCGAAA CAGCAT-3′; FAM-probe: 5′-FAM/CTGCAGTCC/ZEN/CTCCTG CTTAGGGTCG-3′). The retrovirus parent plasmid was used to generate the standard curves.

Data Availability

The raw data supporting the findings of this study are available from the corresponding authors (D.M.S. or J.H.B.) upon request.

Materials Availability

Materials are available under a material transfer agreement (MTA).

Statistics

Data are represented as mean ± SEM. One-way ANOVA followed by Bonferroni multiple comparison test was used to compare multiple treatment groups. Two-way ANOVA followed by Bonferroni test was used to assess statistical significance of differences in tumor growth between multiple treatment groups at different time points. Survival was recorded by Kaplan-Meier graphs, with significance determined by the log-rank test. Data were analyzed using GraphPad Prism v.5.0 software (GraphPad, La Jolla, CA).

SUPPLEMENTAL INFORMATION

Supplemental Information includes six figures and can be found with this article online at https://doi.org/10.1016/j.omto.2018.12.009.

AUTHOR CONTRIBUTIONS

M.T.D. designed and performed experiments in each figure and drafted the paper. M.R.C.-P. participated in the design of the project and performed experiments in Figures 1, 2, and S2. E.M., A.L., and K.L.S. performed animal implantations, imaging, and phenotyping. M.Z., M.E.B., and W.-C.C. designed and constructed virus constructs and performed T cell transductions. S.P.S. and S.M.T. designed and assisted in the pharmacologic assessments. K.M.S. and A.E.F. designed and supervised aspects of the project. D.M.S. and J.H.B. designed and supervised the experiments and wrote the paper.

CONFLICTS OF INTEREST

All authors were employees of Bellicum when the work was completed and have financial interests in the company. Moreover, K.M.S. and D.M.S. are cofounders of Bellicum. M.T.D., M.R.C.-P., A.E.F., D.M.S., K.M.S., and J.H.B. have patent applications surrounding the findings of this study.

ACKNOWLEDGMENTS

The authors thank Tom Farrell, Tsvetelina Hoang, Aruna Mahendravada, and Nick Shinners for helpful discussions; Margie Harris for technical assistance; and William Grossman and Greg Naeve for careful editing and discussions. This work was internally funded.

REFERENCES

1. Davila, M.L., Riviere, I., Wang, X., Bartido, S., Park, J., Curran, K., Chung, S.S., Stefanski, J., Borquez-Ojeda, O., Olszewska, M., et al. (2014). Efficacy and toxicity management of 19-28z CAR T cell therapy in B cell acute lymphoblastic leukemia. Sci. Transl. Med. *6*, 224ra25.
2. Turtle, C.J., Hanafi, L.A., Berger, C., Gooley, T.A., Cherian, S., Hudecek, M., Sommermeyer, D., Melville, K., Pender, B., Budiarto, T.M., et al. (2016). CD19 CAR-T cells of defined CD4+:CD8+ composition in adult B cell ALL patients. J. Clin. Invest. *126*, 2123–2138.
3. Grupp, S.A., Kalos, M., Barrett, D., Aplenc, R., Porter, D.L., Rheingold, S.R., Teachey, D.T., Chew, A., Hauck, B., Wright, J.F., et al. (2013). Chimeric antigen receptor-modified T cells for acute lymphoid leukemia. N. Engl. J. Med. *368*, 1509–1518.
4. Park, J.H., Rivière, I., Gonen, M., Wang, X., Sénéchal, B., Curran, K.J., Sauter, C., Wang, Y., Santomasso, B., Mead, E., et al. (2018). Long-Term Follow-up of CD19 CAR Therapy in Acute Lymphoblastic Leukemia. N. Engl. J. Med. *378*, 449–459.
5. Schuster, S.J., Svoboda, J., Chong, E.A., Nasta, S.D., Mato, A.R., Anak, Ö., Brogdon, J.L., Pruteanu-Malinici, I., Bhoj, V., Landsburg, D., et al. (2017). Chimeric Antigen Receptor T Cells in Refractory B-Cell Lymphomas. N. Engl. J. Med. *377*, 2545–2554.
6. Neelapu, S.S., Locke, F.L., Bartlett, N.L., Lekakis, L.J., Miklos, D.B., Jacobson, C.A., Braunschweig, I., Oluwole, O.O., Siddiqi, T., Lin, Y., et al. (2017). Axicabtagene Ciloleucel CAR T-Cell Therapy in Refractory Large B-Cell Lymphoma. N. Engl. J. Med. *377*, 2531–2544.
7. Berdeja, J.G., Lin, Y., Raje, N., Munshi, N., Siegel, D., Liedtke, M., Jagannath, S., Maus, M.V., Turka, A., Lam, L.P., et al. (2017). Durable Clinical Responses in Heavily Pretreated Patients with Relapsed/Refractory Multiple Myeloma: Updated Results from a Multicenter Study of bb2121 Anti-Bcma CAR T Cell Therapy. Blood *130*, 740.
8. Ahmed, N., Brawley, V.S., Hegde, M., Robertson, C., Ghazi, A., Gerken, C., Liu, E., Dakhova, O., Ashoori, A., Corder, A., et al. (2015). Human Epidermal Growth Factor Receptor 2 (HER2) -Specific Chimeric Antigen Receptor-Modified T Cells for the Immunotherapy of HER2-Positive Sarcoma. J. Clin. Oncol. *33*, 1688–1696.
9. Yazdanifar, M., Zhou, R., and Mukherjee, P. (2016). Emerging immunotherapeutics in adenocarcinomas: A focus on CAR-T cells. Curr. Trends Immunol. *17*, 95–115.
10. Sidaway, P. (2017). Immunotherapy: Glioblastoma regression obtained with CAR T cells. Nat. Rev. Clin. Oncol. *14*, 138.
11. Maus, M.V., and June, C.H. (2016). Making Better Chimeric Antigen Receptors for Adoptive T-cell Therapy. Clin. Cancer Res. *22*, 1875–1884.
12. Sun, J., and Sadelain, M. (2015). The quest for spatio-temporal control of CAR T cells. Cell Res. *25*, 1281–1282.
13. Lim, W.A., and June, C.H. (2017). The Principles of Engineering Immune Cells to Treat Cancer. Cell *168*, 724–740.
14. Sadelain, M., Brentjens, R., and Rivière, I. (2013). The basic principles of chimeric antigen receptor design. Cancer Discov. *3*, 388–398.
15. Sadelain, M., Rivière, I., and Riddell, S. (2017). Therapeutic T cell engineering. Nature *545*, 423–431.
16. Zhong, X.S., Matsushita, M., Plotkin, J., Riviere, I., and Sadelain, M. (2010). Chimeric antigen receptors combining 4-1BB and CD28 signaling domains augment PI3kinase/AKT/Bcl-XL activation and CD8+ T cell-mediated tumor eradication. Mol. Ther. *18*, 413–420.
17. Foster, A.E., Mahendravada, A., Shinners, N.P., Chang, W.C., Crisostomo, J., Lu, A., Khalil, M., Morschl, E., Shaw, J.L., Saha, S., et al. (2017). Regulated Expansion and

Survival of Chimeric Antigen Receptor-Modified T Cells Using Small Molecule-Dependent Inducible MyD88/CD40. Mol. Ther. *25*, 2176–2188.

18. Lyddane, C., Gajewska, B.U., Santos, E., King, P.D., Furtado, G.C., and Sadelain, M. (2006). Cutting Edge: CD28 controls dominant regulatory T cell activity during active immunization. J. Immunol. *176*, 3306–3310.
19. Milone, M.C., Fish, J.D., Carpenito, C., Carroll, R.G., Binder, G.K., Teachey, D., Samanta, M., Lakhal, M., Gloss, B., Danet-Desnoyers, G., et al. (2009). Chimeric receptors containing CD137 signal transduction domains mediate enhanced survival of T cells and increased antileukemic efficacy in vivo. Mol. Ther. *17*, 1453–1464.
20. Kalos, M., Levine, B.L., Porter, D.L., Katz, S., Grupp, S.A., Bagg, A., and June, C.H. (2011). T cells with chimeric antigen receptors have potent antitumor effects and can establish memory in patients with advanced leukemia. Sci. Transl. Med. *3*, 95ra73.
21. Maude, S.L., Frey, N., Shaw, P.A., Aplenc, R., Barrett, D.M., Bunin, N.J., Chew, A., Gonzalez, V.E., Zheng, Z., Lacey, S.F., et al. (2014). Chimeric antigen receptor T cells for sustained remissions in leukemia. N. Engl. J. Med. *371*, 1507–1517.
22. Narayanan, P., Lapteva, N., Seethammagari, M., Levitt, J.M., Slawin, K.M., and Spencer, D.M. (2011). A composite MyD88/CD40 switch synergistically activates mouse and human dendritic cells for enhanced antitumor efficacy. J. Clin. Invest. *121*, 1524–1534.
23. Mata, M., Gerken, C., Nguyen, P., Krenciute, G., Spencer, D.M., and Gottschalk, S. (2017). Inducible Activation of MyD88 and CD40 in CAR T Cells Results in Controllable and Potent Antitumor Activity in Preclinical Solid Tumor Models. Cancer Discov. *7*, 1306–1319.
24. Spencer, D.M., Wandless, T.J., Schreiber, S.L., and Crabtree, G.R. (1993). Controlling signal transduction with synthetic ligands. Science *262*, 1019–1024.
25. Clackson, T., Yang, W., Rozamus, L.W., Hatada, M., Amara, J.F., Rollins, C.T., Stevenson, L.F., Magari, S.R., Wood, S.A., Courage, N.L., et al. (1998). Redesigning an FKBP-ligand interface to generate chemical dimerizers with novel specificity. Proc. Natl. Acad. Sci. USA *95*, 10437–10442.
26. Kemnade, J.O., Seethammagari, M., Narayanan, P., Levitt, J.M., McCormick, A.A., and Spencer, D.M. (2012). Off-the-shelf adenoviral-mediated immunotherapy via bicistronic expression of tumor antigen and iMyD88/CD40 adjuvant. Mol. Ther. *20*, 1462–1471.
27. Di Stasi, A., Tey, S.K., Dotti, G., Fujita, Y., Kennedy-Nasser, A., Martinez, C., Straathof, K., Liu, E., Durett, A.G., Grilley, B., et al. (2011). Inducible apoptosis as a safety switch for adoptive cell therapy. N. Engl. J. Med. *365*, 1673–1683.
28. Spencer, D.M., Belshaw, P.J., Chen, L., Ho, S.N., Randazzo, F., Crabtree, G.R., and Schreiber, S.L. (1996). Functional analysis of Fas signaling in vivo using synthetic inducers of dimerization. Curr. Biol. *6*, 839–847.
29. Straathof, K.C., Pulè, M.A., Yotnda, P., Dotti, G., Vanin, E.F., Brenner, M.K., Heslop, H.E., Spencer, D.M., and Rooney, C.M. (2005). An inducible caspase 9 safety switch for T-cell therapy. Blood *105*, 4247–4254.
30. Zhou, X., Di Stasi, A., Tey, S.K., Krance, R.A., Martinez, C., Leung, K.S., Durett, A.G., Wu, M.F., Liu, H., Leen, A.M., et al. (2014). Long-term outcome after haploidentical stem cell transplant and infusion of T cells expressing the inducible caspase 9 safety transgene. Blood *123*, 3895–3905.
31. Diaconu, I., Ballard, B., Zhang, M., Chen, Y., West, J., Dotti, G., and Savoldo, B. (2017). Inducible Caspase-9 Selectively Modulates the Toxicities of CD19-Specific Chimeric Antigen Receptor-Modified T Cells. Mol. Ther. *25*, 580–592.
32. Fan, L., Freeman, K.W., Khan, T., Pham, E., and Spencer, D.M. (1999). Improved artificial death switches based on caspases and FADD. Hum. Gene Ther. *10*, 2273–2285.
33. Sabatini, D.M., Erdjument-Bromage, H., Lui, M., Tempst, P., and Snyder, S.H. (1994). RAFT1: a mammalian protein that binds to FKBP12 in a rapamycin-dependent fashion and is homologous to yeast TORs. Cell *78*, 35–43.
34. Brown, E.J., Albers, M.W., Shin, T.B., Ichikawa, K., Keith, C.T., Lane, W.S., and Schreiber, S.L. (1994). A mammalian protein targeted by G1-arresting rapamycin-receptor complex. Nature *369*, 756–758.
35. Kunz, J., Henriquez, R., Schneider, U., Deuter-Reinhard, M., Movva, N.R., and Hall, M.N. (1993). Target of rapamycin in yeast, TOR2, is an essential phosphatidylinositol kinase homolog required for G1 progression. Cell *73*, 585–596.
36. Chen, J., Zheng, X.F., Brown, E.J., and Schreiber, S.L. (1995). Identification of an 11-kDa FKBP12-rapamycin-binding domain within the 289-kDa FKBP12-rapamycin-associated protein and characterization of a critical serine residue. Proc. Natl. Acad. Sci. USA *92*, 4947–4951.
37. Ho, S.N., Biggar, S.R., Spencer, D.M., Schreiber, S.L., and Crabtree, G.R. (1996). Dimeric ligands define a role for transcriptional activation domains in reinitiation. Nature *382*, 822–826.
38. Bayle, J.H., Grimley, J.S., Stankunas, K., Gestwicki, J.E., Wandless, T.J., and Crabtree, G.R. (2006). Rapamycin analogs with differential binding specificity permit orthogonal control of protein activity. Chem. Biol. *13*, 99–107.
39. Rivera, V.M., Clackson, T., Natesan, S., Pollock, R., Amara, J.F., Keenan, T., Magari, S.R., Phillips, T., Courage, N.L., Cerasoli, F., Jr., et al. (1996). A humanized system for pharmacologic control of gene expression. Nat. Med. *2*, 1028–1032.
40. Stankunas, K., Bayle, J.H., Gestwicki, J.E., Lin, Y.M., Wandless, T.J., and Crabtree, G.R. (2003). Conditional protein alleles using knockin mice and a chemical inducer of dimerization. Mol. Cell *12*, 1615–1624.
41. Stankunas, K., Bayle, J.H., Havranek, J.J., Wandless, T.J., Baker, D., Crabtree, G.R., and Gestwicki, J.E. (2007). Rescue of degradation-prone mutants of the FK506-rapamycin binding (FRB) protein with chemical ligands. ChemBioChem *8*, 1162–1169.
42. Shultz, L.D., Lyons, B.L., Burzenski, L.M., Gott, B., Chen, X., Chaleff, S., Kotb, M., Gillies, S.D., King, M., Mangada, J., et al. (2005). Human lymphoid and myeloid cell development in NOD/LtSz-scid IL2R gamma null mice engrafted with mobilized human hemopoietic stem cells. J. Immunol. *174*, 6477–6489.
43. Iuliucci, J.D., Oliver, S.D., Morley, S., Ward, C., Ward, J., Dalgarno, D., Clackson, T., and Berger, H.J. (2001). Intravenous safety and pharmacokinetics of a novel dimerizer drug, AP1903, in healthy volunteers. J. Clin. Pharmacol. *41*, 870–879.
44. O'Rourke, D.M., Nasrallah, M.P., Desai, A., Melenhorst, J.J., Mansfield, K., Morrissette, J.J.D., Martinez-Lage, M., Brem, S., Maloney, E., Shen, A., et al. (2017). A single dose of peripherally infused EGFRvIII-directed CAR T cells mediates antigen loss and induces adaptive resistance in patients with recurrent glioblastoma. Sci. Transl. Med. *9*, eaaa0984.
45. Morello, A., Sadelain, M., and Adusumilli, P.S. (2016). Mesothelin-Targeted CARs: Driving T Cells to Solid Tumors. Cancer Discov. *6*, 133–146.
46. Heczey, A., Louis, C.U., Savoldo, B., Dakhova, O., Durett, A., Grilley, B., Liu, H., Wu, M.F., Mei, Z., Gee, A., et al. (2017). CAR T Cells Administered in Combination with Lymphodepletion and PD-1 Inhibition to Patients with Neuroblastoma. Mol. Ther. *25*, 2214–2224.
47. Louis, C.U., Savoldo, B., Dotti, G., Pule, M., Yvon, E., Myers, G.D., Rossig, C., Russell, H.V., Diouf, O., Liu, E., et al. (2011). Antitumor activity and long-term fate of chimeric antigen receptor-positive T cells in patients with neuroblastoma. Blood *118*, 6050–6056.
48. Tey, S.K., Dotti, G., Rooney, C.M., Heslop, H.E., and Brenner, M.K. (2007). Inducible caspase 9 suicide gene to improve the safety of allodepleted T cells after haploidentical stem cell transplantation. Biol. Blood Marrow Transplant. *13*, 913–924.
49. Knochelmann, H.M., Smith, A.S., Dwyer, C.J., Wyatt, M.M., Mehrotra, S., and Paulos, C.M. (2018). CAR T Cells in Solid Tumors: Blueprints for Building Effective Therapies. Front. Immunol. *9*, 1740.
50. Jones, B.S., Lamb, L.S., Goldman, F., and Di Stasi, A. (2014). Improving the safety of cell therapy products by suicide gene transfer. Front. Pharmacol. *5*, 254.
51. Philip, B., Kokalaki, E., Mekkaoui, L., Thomas, S., Straathof, K., Flutter, B., Marin, V., Marafioti, T., Chakraverty, R., Linch, D., et al. (2014). A highly compact epitope-based marker/suicide gene for easier and safer T-cell therapy. Blood *124*, 1277–1287.
52. Tasian, S.K., Kenderian, S.S., Shen, F., Ruella, M., Shestova, O., Kozlowski, M., Li, Y., Schrank-Hacker, A., Morrissette, J.J.D., Carroll, M., et al. (2017). Optimized depletion of chimeric antigen receptor T cells in murine xenograft models of human acute myeloid leukemia. Blood *129*, 2395–2407.
53. Stavrou, M., Philip, B., Traynor-White, C., Davis, C.G., Onuoha, S., Cordoba, S., Thomas, S., and Pule, M. (2018). A Rapamycin-Activated Caspase 9-Based Suicide Gene. Mol. Ther. *26*, 1266–1276.
54. Liberles, S.D., Diver, S.T., Austin, D.J., and Schreiber, S.L. (1997). Inducible gene expression and protein translocation using nontoxic ligands identified by a mammalian three-hybrid screen. Proc. Natl. Acad. Sci. USA *94*, 7825–7830.